# Record Low NEP in the Hot-Electron Titanium Nanobolometers

Boris S. Karasik[#], David Olaya, Jian Wei, Sergey Pereverzev, Michael E. Gershenson, Jonathan H. Kawamura, William R. McGrath, and Andrei V. Sergeev

***Abstract*—We are developing hot-electron superconducting transition-edge sensors (TES) capable of counting THz photons and operating at $T = 0.3$K. We fabricated superconducting Ti nanosensors with Nb contacts with a volume of ~ $3\times10^{-3}$ μm$^3$ on planar Si substrate and have measured the thermal conductance due to the weak electron-phonon coupling in the material $G = 4\times10^{-14}$ W/K at 0.3 K. The corresponding phonon-noise $NEP = 3\times10^{-19}$ W/Hz$^{1/2}$. Detection of single optical photons (1550nm and 670nm wavelength) has been demonstrated for larger devices and yielded the thermal time constants of 30 μs at 145 mK and of 25 μs at 190 mK. This Hot-Electron Direct Detector (HEDD) is expected to have a sufficient energy resolution for detecting individual photons with $\nu > 1$ THz where NEP ~ $3\times10^{-20}$ W/Hz$^{1/2}$ is needed for spectroscopy in space.**

***Index Terms*—radiation detectors, submillimeter wave detectors, bolometers, superconducting devices**

## I. Introduction

SEVERAL advanced space submillimeter astronomy missions (SAFIR [1,2], SPECS [3],SPICA [4]) have been recently proposed. These missions would make a dramatic impact on the achievable sensitivity in the spectrometer with moderate resolution ($R = \nu/\Delta\nu \sim 1000$) due to active cooling of telescope mirrors down to ~ 4 K. This deep cooling would significantly reduce the telescope emissivity and enable realization of the background-limited noise equivalent power (*NEP*) ~ $10^{-19}$-$10^{-20}$ W/Hz$^{1/2}$ at submillimeter wavelengths (see Fig. 1). However, the *NEP* of state-of-the-art direct detectors [2,5] needs to be lowered by almost two orders of magnitude to meet this goal. The membrane supported bolometers have come close to meeting the sensitivity goals [6]: a low phonon conductance has been achieved in long (~ 1-8 mm) $Si_3N_4$ beams suggesting an *NEP* < $10^{-19}$ W/Hz$^{1/2}$ in the 50-100 mK temperature range. The further decrease of the thermal conductance is hindered by the weakening of the temperature dependence of the thermal conductance due to transition to the 1-D phonon transport.

Besides the more traditional photon-integrating mode of operation, a photon counting mode may be required to achieve the lowest *NEP*. Background-limited operation above 1 THz would correspond to a very low photon arrival rate [7]:

$$N_{ph} = \frac{1}{2}\left(\eta\frac{NEP}{h\nu}\right)^2 < 100 \text{ s}^{-1}, \qquad (1)$$

($\eta$ is the optical coupling efficiency). A detector with a time constant $\tau$ will integrate a photon flux if $N_{ph}\tau >> 1$. Therefore, a background limited integrating detector must have a time constant of 0.1 s or greater. Such a long time constant is problematic for many detector concepts: typically, $\tau$ does not exceed a few milliseconds for hot-electron detectors and kinetic inductance detectors, so they both would have to operate in the photon counting mode for the detection of weak signals. Although the photon counting mode in the THz range has been considered in several papers (see, e.g., [7,8,9]), the detection of individual THz photons has been demonstrated only using the quantum-dot devices [10]. The latter approach has been recently advanced towards practical application in terahertz microscopy [11].

## II. Thermal conductance and expected NEP

We are pursuing a Hot-Electron Direct Detector (= hot-electron TES), which can operate in both photon-integrating and photon-counting modes at 0.3 K [12]. The idea of improving the sensitivity of bolometers by employing the hot-electron effects at ultra-low temperatures has been developed by several groups over a number of years [12,13,14,15,16]. The fundamental limit of the *NEP* is set in this case by the thermal energy fluctuations:

$$NEP = \sqrt{2k_B T_e^2\, C_e\left(T_e, V\right)\Big/\tau_{e-ph}\left(T_e\right)}\,. \qquad (2)$$

Here $C_e = \gamma V T_e$ is the electron heat capacity, $V$ is the sensor volume, $\gamma$ is the Sommerfeld constant, and $\tau_{e\text{-}ph}$ is the electron-phonon energy relaxation time. The sensitivity increases with decreasing the sensor volume and lowering the electron temperature $T_e$. Especially strong is the effect of lowering $T_e$:

Manuscript received August 28, 2006. (Write the date on which you submitted your paper for review.) The research of BSK, JHK and WRM was carried out at the Jet Propulsion Laboratory, California Institute of Technology, under a contact with the National Aeronautics and Space Administration. The work at Rutgers University was supported in part by the NASA grant NNG04GD55G and the Rutgers Academic Excellence Fund.

B. Karasik, J. Kawamura, and W. McGrath are with the Jet Propulsion Laboratory, California Institute of Technology, Pasadena, CA 91109, USA.

D. Olaya, J. Wei, S. Pereverzev and M. Gershenson are with Rutgers University, Piscataway, NJ 08854, USA.

A. Sergeev is with SUNY ay Buffalo, Buffalo, NY 14260.

[#] Corresponding author. Phone: 818-393-4438,
email: boris.s.karasik@jpl.nasa.gov

$NEP_{\text{e-ph}} \sim T_e^{7/2}$ because of a very rapid increase of the electron-

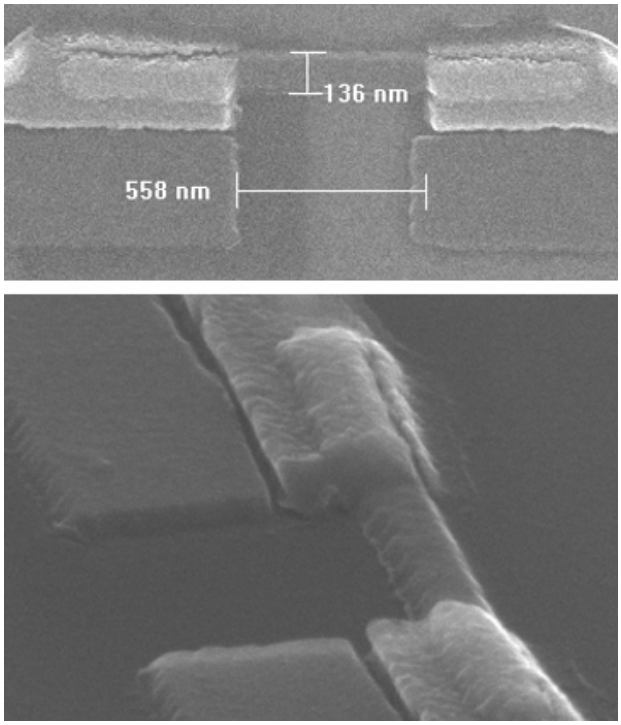


Fig. 2. SEM image of a Ti nanosensor. Top view: the Ti nanosensor with dimensions 0.04μm × 0.14μm × 0.56μm is flanked by Nb current leads (Ti is dark gray and Nb is light gray). The rest of Ti film is separated from the Ti nanosensor and Nb leads by trenches, which are clearly seen on the bottom microphotograph taken at an angle.

phonon relaxation time $\tau_{\text{e-ph}} \propto T_e^{-4}$ in disordered conductors at ultra-low temperatures (see, e.g., [17,18]). Since the electron temperature is always ~ $T_C$ in hot-electron TES, then lowering $T_e$ requires reducing $T_C$ to the desired level. This can be achieved by magnetic ion implantation, e.g. $^{+}Mn^{55}$ ions work well on Ti [19]. Using conventional nanolithographic methods, the volume of metallic nanostructures can be reduced down to ~$10^{-21}$ m$^3$, which translates into $C_e(0.3\text{ K}) \sim 10^{-19}$ J/K. For such a nanosensor, the predicted *NEP* can be $10^{-19}$ W/Hz$^{1/2}$ at $T \approx 0.3$ K and $10^{-20}$ W/Hz$^{1/2}$ at $T \approx 0.1$ K [12]. However, even a record long $\tau_{e\text{-}ph} \sim 20$ ms measured in thin Hf and Ti films at 40 mK [18] is insufficiently long for integrating photons with $N_{ph} \sim 100$ s$^{-1}$.

Equation (2) assumes that the electron-phonon relaxation is the only mechanism of energy dissipation. To prevent the energy flow from the antenna-coupled nanosensor, the electrical leads to the nanostructure should be made of a superconductor with a sufficiently large superconducting gap: in this case, while electrical current can freely flow across the normal metal-superconductor interface, the outdiffusion of "hot" electrons is blocked by Andreev reflection. The detector design should also ensure the suppression of photon emission by electrons in the frequency range corresponding to the operating temperature 0.3K (~ 10 GHz) [20]; this, however, can be achieved simultaneously with a good impedance match between the sensor and the embedded circuit.

We have been systematically working on the realization of ultra-sensitive HEDDs for a number of years [12,18,21,22] and recently achieved the expected thermal characteristics in nanoscale Ti HEDDs with Nb contacts.

The HEDD element is a transition edge nanosensor made from thin Ti film with superconducting transition temperature $T_C$~0.2-0.4 K. The current leads to the nanosensor are fabricated from Nb films with $T_C \sim 8.5$ K; a large superconducting gap in Nb blocks outdiffusion of "hot" electrons into the current leads. The nanostructure is fabricated on a silicon substrate using electron-beam lithography and e-beam deposition of Ti and Nb. For fabrication of an oxide-free Ti/Nb interface, we used the so-called "shadow mask" technique: Ti and Nb films were sequentially deposited at different angles through a "shadow" mask without breaking vacuum. The fabrication procedure is similar to that used in our previous paper [23].

A Ti device with typical dimensions is shown in Fig. 2. Among different tested devices the normal-state resistance ranges between 50-100 Ohm and the critical temperature is within 0.1-0.4 K. The minimum device width is set by the e-beam lithography. Further reduction of the device length should be done with caution: for nanosensors with length comparable to the thermal length $L_C = \sqrt{\hbar D / k_B T}$, where $D$ is the diffusion constant, the superconducting transition temperature will may be significantly increased due to the proximity effect between Ti nanosensor and Nb current leads if the Nb/Ti interface has good transparency. For the studied Ti films with diffusion constant $D \sim 4$ cm$^2$/s, $L_C$ is of the order of 0.1 μm at $T = 0.3$K. Also, if the length of the Ti nanosensor is smaller than the electron thermalization length, the frequency-dependent response and drop in sensitivity might be expected at $h\nu > \Delta$Nb ($\nu > 0.3$ THz). For this reason we do did not make HEDD devices shorter than ~ 0.5 μm.

Measurements of the thermal conductance $G$ have been performed in the dilution refrigerator equipped with several stages of low-pass electical filters thermally anchored to the 1K pot and mixing chamber; the filters were designed to suppress both the low-frequency interferences and rf noise over the frequency range from kHz to several GHz. Because of high sensitivity, the devices can be overheated above their superconducting transition temperature by electromagnetic noise with the power $\delta T_C C_e / \tau_{e\text{-}ph} \le 1$ fW.

Fig. 3 illustrates the measurement of the thermal conductance $G = C_e / \tau_{e\text{-}ph}$ between the electrons in a nanosensor and the thermal bath. The resistance of devices was measured by an AC (13 Hz) resistance bridge using a small (typically, 0.1-1 nA) measuring current. The Ti nanosensor was slightly heated by a DC current, and the difference between the electron temperature $T_e$ and the equilibrium bath temperature $T_{ph}$ was determined by observing the temperature shift of the superconducting transition. This method assumes that the non-equilibrium electron distribution function can be characterized with an effective electron temperature. This assumption is valid at sub-Kelvin temperatures, where the electron-electron scattering rate in thin films exceeds by many orders of magnitude the electron-phonon scattering rate [13]. To measure $G$ at $T < T_C$ the

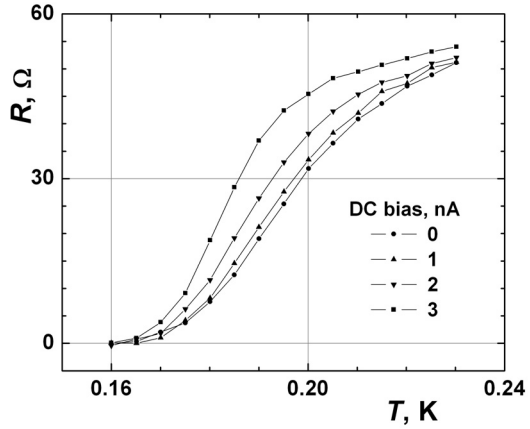


Fig. 3. Measurements of the thermal conductivity between the electrons in a Ti HEDD device with dimensions 0.04μm × 0.14μm × 0.56μm and the thermal bath. The shift of the superconducting transition is caused by the Joule heat generated in the sample by the DC bias current.

superconducting transition was suppressed to lower temperatures by applying a magnetic field perpendicular to the plane of the nanosensor. The thermal conductivity was found from the balance equation:

$$RI_{DC}^2 = G(T_e)(T_e - T_{ph}), \qquad (3)$$

which holds if $T_e - T_{ph} << T_{ph}$. For the device with dimensions 0.04μm × 0.14μm × 0.56μm and $T_C \approx 0.3$ K, we obtained $G(0.3\text{K}) = 4\times10^{-14}$ W/K. According to Eq. 2, this would correspond to the phonon-noise $NEP = 3\times10^{-19}$ W/Hz$^{1/2}$.

The value of $G$ normalized to volume $G(0.3\text{K})/V = 1.2\times10^{7}$ W/(K·m$^3$) agrees very well with the corresponding value of $G/V$ measured for much larger meander-patterned Ti films with dimensions 0.04μm × 5μm × 100,000μm (note that the length of 10 cm for the latter structures is much greater than the diffusion length over the electron-phonon relaxation time, $L_{e-ph} = (D\tau_{e\text{-}ph})^{1/2}$). The scaling of $G$ with the sensor volume (over 6 orders of magnitude) provides an experimental proof that in both types of structures, the nanostructures with superconducting contacts and much larger Ti meanders, the dominant mechanism of energy dissipation at $T = 0.3$K is electron-phonon scattering, and that the energy relaxation due to outdiffusion of hot electrons can be neglected. The measured values of $G(0.3\text{K})$ are in reasonable agreement with the estimate of $G$ on the basis of the theory of electron-phonon energy relaxation in disordered conductors [17] and our previous measurements of the electron-phonon relaxation rate in disordered Ti films [18].

## III. Detection of Single Optical/NIR Photons and the Time Constant

Knowing the time constant is important for estimation of the HEDD operation in the photon-counting mode since it determines both the dynamic range and the energy resolution. We found the thermal time constant ($\approx \tau_{e\text{-}ph}$) experimentally by measuring the response of the HEDD device to single optical (670nm) and NIR (1550nm) photons. The heavily attenuated (50dB at 4K, 0-30 dB at room temperature) optical radiation from either a cw (670nm) or a pulse-modulated (1550nm) laser was sent into the dilution refrigerator via an optical fiber. The current signal was measured using a dc SQUID with a ~ 100kHz bandwidth.

The submicron devices used for the thermal conductance measurements were too small for this purpose, that is, the electron temperature rise after detection of a photon $\Delta T_e = h\nu/C_e$ would be too large compared to $\delta T_C$. That would cause a switch of the device from superconducting to the normal state and, thus, a non-linear relaxation. We fabricated much larger devices of two types: one type consisted of 10 parallel 10-μm-long Ti strips with the same Nb contact configuration as shown in Fig. 2; another type was a 20-μm-long single Ti strip with Nb contacts.

The critical temperature in a 10-strip device was 145 mK. Fig. 4 shows the current-voltage characteristics (IV's) and the current responsivity in such a device measured at different temperatures. Well below $T_C$, the IV curves demonstrate a branch with the negative differential resistance where the electro-thermal feedback (ETF) should be strong. In this case, the dc resistance in the operating point was very low. The shapes of the responsivity curves are consistent with the bolometric models taking into account the ETF effect.

Fig. 5 shows single photon pulses of both wavelengths. As expected, the amplitudes of the pulses are approximately inversely proportional to the wavelength. That is an indication that the response is sufficiently linear, that is, the heat capacity of the device is large enough and $\Delta T_e$ is smaller than $\delta T_C$. The pulse decay was found to be practically exponential with the time constant $\approx 30$ μs, which did not depend on the bath temperature. It is not surprising since the bias conditions were adjusted for each temperature to maximize the response and, thus, the electron temperature was always within the $\delta T_C$ interval.

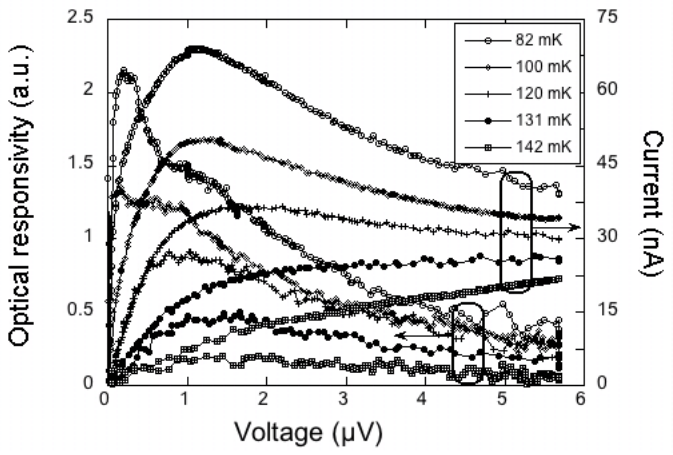


Fig. 4. The current-voltage characteristics and the relative current responsivity of a 10-strip device used for optical measurements as functions of temperature.

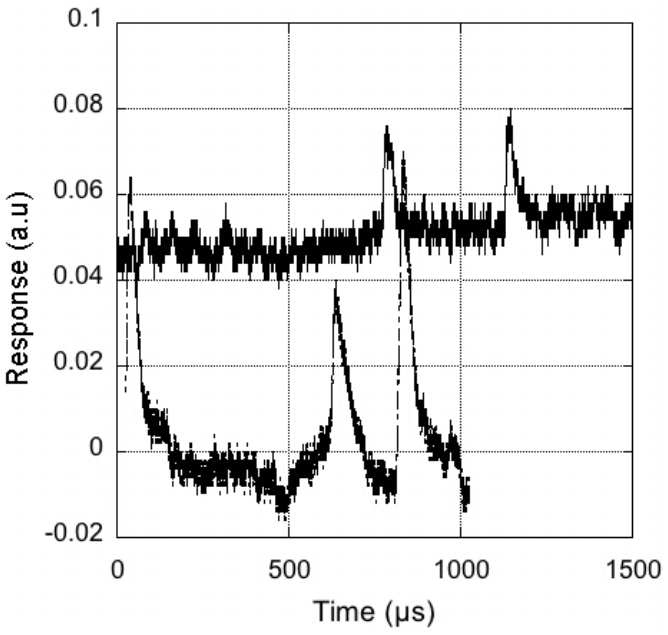


Fig. 5. Single-photon detection with a 10-strip HEDD device. Upper trace: 1550 nm single-photon responses; lower trace: 670 nm single-photon responses. The vertical scale is the same for both traces. The traces are vertically offset for clarity. The measurement temperature was 50 mK.

Similar measurements using $\lambda = 1550$ nm were done also on a single-strip 20-μm-long device with a critical temperature of ≈ 190 mK yielding the time constant ≈ 25 μs. Taking a bulk value of the Sommerfeld constant for Ti $\gamma = 316$ J/(K$^2$·m$^3$) and $G(0.3\text{K})/V = 1.2\times10^7$ W/(K·m$^3$) found in Sec. II, one can derive the expected time constant at 0.3 K to be 8 μs (the corresponding value of $C_e/G$ from [18] was 20 μs; this discrepancy is being addressed in the on-going work). This time constant derived from the thermal conductance measurements is shorter than the values measured optically but this can be expected given some power-law temperature dependence of the electron-phonon relaxation time. Assuming that the material properties for all the studied in this work devices are identical, the electron-phonon relaxation time should have follow the temperature dependence: $\tau_{e\text{-}ph} \sim T^{-n}$, with $n = 2\pm0.3$.

## IV. Photon Counting Mode

Although some clarification of the time constant and its temperature dependence is needed, it is unlikely that the Sommerfeld constant in small HEDD devices is much different from the bulk value. In this Section we model the expected performance of the HEDD in the THz photon counting model basing on the achieved device dimensions, operating temperature and superconducting transition width.

The photon counting device would operate in the voltage-biased TES mode; that is, its operating temperature will be somewhat lower than $T_C$, and the resistance at the operating point, $R$, will be much smaller than the normal resistance $R_N$ similar to the bias conditions for the above optical measurements. This biasing mode enables the device to simultaneously match to the THz antenna impedance and couple well to the SQUID. Indeed, if the DC resistance at the operating point is ~ 1 Ω, the device Johnson noise would exceed the noise of a typical DC SQUID; at the same time, a much higher impedance of the device in the THz range (~ 50-100 Ω) facilitates coupling of the device to a planar antenna. The signal photon will be absorbed increasing the electron temperature in the nanosensor. The increase in electron temperature will cause the current to decrease, and this will be registered by a SQUID readout. The response time of the HEDD devices is controlled by the electron-phonon energy relaxation time $\tau_{e\text{-}ph}$ (~8 μs at 0.3K). The actual response time may be significantly shorter due to the negative electrothermal feedback (ETF) effect [24]: $\tau = \tau_{e\text{-}ph}/(1+L)$, where $L$ is the ETF loop gain.

The energy resolution in this mode is defined by the effective noise bandwidth due to the presence of the thermal energy fluctuations and the Johnson noise [24] and is given by:

$$\delta E = \left(4\sqrt{n/2}\, k_B T_e^2 C_e / \alpha\right)^{1/2}. \qquad (4)$$

Here $\alpha = \partial \ln R/\partial \ln T$ ($= 2T_C/\delta T_C \approx 60$ for our best samples), $n = 5$-6 is the exponent in the electron-phonon thermal conductance. For a practical device with minimal dimensions 0.04μm × 0.1μm × 0.5μm, the estimated energy resolution, $\delta E$, corresponds to the "red boundary" $\nu_R = \delta E/h = 0.17$ THz. The value of $N_{max} \approx \tau^{-1}$ [7] determines the maximum count rate; this value can be as large as ~ $1\times10^6$ s$^{-1}$ at $T = 0.3$K. This would provide a large dynamic range for the counter: $N_{max}/N_{ph}^{1/2} \sim 50$ dB ( $N_{ph}^{1/2}$ is the minimum signal which can be distinguished from the background).

In order to achieve the background-limited performance, the

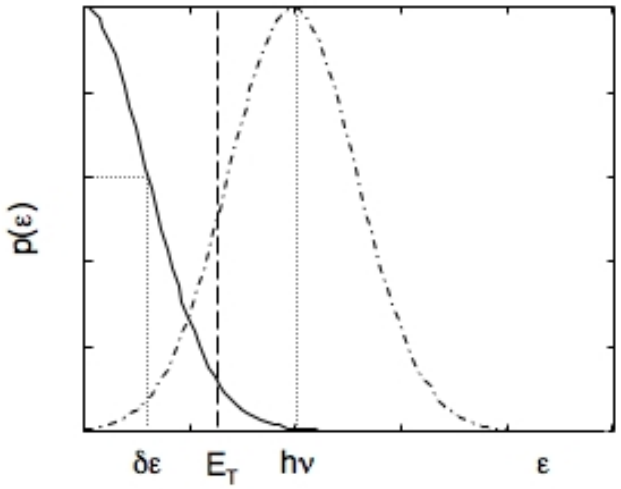


Fig. 6. The trade-off between the intrinsic quantum efficiency and the dark count rate. Solid bell-shaped line is the Gaussian distribution of the noise as function of energy $\varepsilon$ with $\delta\varepsilon$ as the standard deviation. Dashed-dotted line indicates the same distribution shifted by $h\nu$. The dashed line is the threshold ($E_T$) discriminating the device noise from the detection events. The probability of the dark counts is the area of the *solid curve above* $E_T$ (very small in the figure). The intrinsic quantum efficiency is the area of the *dashed-dotted curve above* $E_T$. Good discrimination roughly corresponds to $h\nu/\delta\varepsilon \approx 6$ with $E_T$ being set in between.

dark count rate due to the device noise, $N_d$, must be lower than $N_{ph}$. The fundamental dark counts are caused by spikes in the device phonon noise that can be mistaken for the signal. To avoid this, an appropriate level of the discrimination threshold, $E_T < h\nu$, must be chosen for the photon counter (see Fig. 6). Setting $E_T$ too high may reduce the intrinsic quantum efficiency of the detector: the photon remains undetected if the sum of a negative noise spike and a positive signal caused by an absorbed photon is lower than the threshold. The analysis based on the Gaussian noise statistics [7] shows that for $\nu = 1$ THz setting $E_T \approx 3.5\delta E$ provides both intrinsic quantum efficiency ≈ 100% and $NEP < 10^{-20}$ W/Hz$^{1/2}$.

## V. Conclusion

We have demonstrated a feasibility of the superconducting Hot-Electron Direct Detector with a record-low $NEP = 3\times10^{-19}$ W/Hz$^{1/2}$ at 0.3 K. This operating temperature can be achieved by He3 sorption cooling; for comparison, similar sensitivity in the conventional bolometers can be realized only at 0.1K or below, which requires dilution refrigeration or adiabatic demagnetization cooling techniques. In its most sensitive photon counting mode, this future detector would be suitable for a background limited spectrometer with moderate resolution ($R$~1000) for space-borne far-IR telescopes with cryogenically cooled mirrors. For higher background applications (e.g., measurements of the Cosmic Microwave Background radiation), HEDD would offer the background limited sensitivity at $T = 0.3$K. The hot-electron detectors have two other important advantages: (a) they are fabricated on bulk substrates, and (b) they have a very short time constant allowing for a high data rate. The HEDDs can be readily matched to a planar antenna since the device RF impedance is in the range 50-100 Ω and the device size is much smaller than the wavelength. As with other transition-edge sensors, the HEDD is compatible with SQUID-based multiplexing read-out circuits

## References


[1] http://safir.jpl.nasa.gov/technologies.shtml.

[2]. D.J. Benford and S.H. Moseley, "Cryogenic detectors for infrared astronomy: the Single Aperture Far-InfraRed (SAFIR) Observatory," *Nucl. Instr. Meth. Phys. Res. A* 520(1-3), 379-383 (2004).

[3]. D. Leisawitz, "NASA's far-IR/submillimeter roadmap missions: SAFIR and SPECS," *Adv. Space Res.* 34(3), 631-636 (2004).

[4]. T. Nakagawa, "SPICA: space infrared telescope for cosmology and astrophysics," *Adv. Space Res.* 34(3), 645-650 (2004).

[5] J.J. Bock, P. Day, A. Goldin, H.G. LeDuc, C. Hunt, A. Lange et al., "Antenna-coupled bolometer array for astrophysics," *Proc. Far-IR, SubMM & MM Detector Technology Workshop, April 1-3, 2002, Monterey, CA*, 224-229.

[6] M. Kenyon, P.K. Day, C.M. Bradford, J.J. Bock, and H.G. Leduc, "Progress on background-limited membrane-isolated TES bolometers for far-IR/submillimeter spectroscopy," *Proc. SPIE*, Vol. 6275, 627508, (2006).

[7] B.S. Karasik and A.V. Sergeev, "THz Hot-Electron Photon Counter," *IEEE Trans. Appl. Supercond*. 15(2), 618-621 (2005).

[8] R.J. Schoelkopf S.H. Moseley, C.M. Stahle, P. Wahlgren, and P. Delsing, "A concept for a submillimeter-wave single-photon counter," *IEEE Trans. Appl. Supercond*. 9(2), Pt.3, 2935-2939 (1999).

[9] A. Semenov, A. Engel, K. Il'in, G. Gol'tsman, M. Siegel and H.W. Hubers, "Ultimate performance of a superconducting quantum detector," *Eur. Phys. J. Appl. Phys.* 21(3), 171-178 (2003).

[10] S. Komiyama, O. Astafiev, V. Antonov, T. Kutsuwa, and H. Hirai, "A single-photon detector in the far-infrared range," *Nature* 403, 405-407 (2000); O. Astafiev, S. Komiyama, T. Kutsuwa, V. Antonov, Y. Kawaguchi, and K. Hirakawa, "Single-photon detector in the microwave range," *Appl. Phys. Lett*. 80(22), 4250-4252 (2002); H. Hashiba, V. Antonov, L. Kulik, S. Komiyama, and C. Stanley, "Highly sensitive detector for submillimeter wavelength range," *Appl. Phys. Lett.* 85(24), 6036-6038 (2004).

[11] K. Ikushima, Y. Yoshimura, T. Hasegawa, S. Komiyama, T. Ueda, and K. Hirakawa, "Photon-counting microscopy of terahertz radiation," *App. Phys. Lett.* 88, 152110 (2006).

[12] B.S. Karasik, W.R. McGrath, M.E. Gershenson, and A.V. Sergeev, "Photon-noise-limited direct detector based on disorder-controlled electron heating," *J. Appl. Phys.* 87(10), 7586-7588 (2000).

[13] E. M. Gershenson, M. E. Gershenson, G. N. Goltsman, A. D. Semenov, and A. V. Sergeev, "Heating of electrons in a superconductor in the resistive state by electromagnetic radiation," *Sov.Phys.-JETP* 59, 442-450 (1984).

[14] M.Nahum and J.M. Martinis, "Ultrasensitive hot-electron microbolometer," *Appl. Phys. Lett*. 63, 3075-3077 (1993).

[15] B. Cabrera, R.M. Clarke, P. Colling, A.J. Miller. S. Nam, R.W. Romani, "Detection of single infrared, optical, and ultraviolet photons using superconducting transition edge sensors," *Appl. Phys. Lett*. 73(6), 735-737 (1998).

[16] T.A Lee, P.L. Richards, S.W. Nam, B. Cabrera, and K.D. Irwin, "A superconducting bolometer with strong electrothermal feedback," *Appl. Phys. Lett.* 69, 1801-1803 (1996).

[17] A. Sergeev and V. Mitin, "Electron-phonon interaction in disordered conductors: Static and vibrating scattering potentials," *Phys. Rev. B.* 61(9), 6041-6047 (2000).

[18] M.E. Gershenson, D. Gong, T. Sato, B.S. Karasik, A.V. Sergeev, "Millisecond electron-phonon relaxation in ultrathin disordered metal films at millikelvin temperatures," *Appl. Phys. Lett*. 79, 2049-2051 (2001).

[19] B.A. Young, J.R. Williams, S.W. Deiker, S.T. Ruggiero, and B. Cabrera, "Using ion implantation to adjust the transition temperature of superconducting films," *Nucl. Inst. Meth. Phys. Res. A* 520, 307-310 (2004).

[20] D.R. Schmidt, R.J. Schoelkopf, and A.N. Cleland, "Photon-Mediated Thermal Relaxation of Electrons in Nanostructures," *Phys. Rev. Lett.* 93, 045901 (2004).

[21] B.S. Karasik, B. Delaet, W.R. McGrath, J. Wei, M.E. Gershenson, and A.V. Sergeev, "Experimental Study of Superconducting Hot-Electron Sensors for Submm Astronomy," *IEEE Trans. Appl. Supercond.* 13(2), 188-191 (2003).

[22] B.S. Karasik, A.V. Sergeyev, D. Olaya, J. Wei, M.E. Gershenson, J.H. Kawamura, and W.R. McGrath, "A Photon Counting Hot-Electron Bolometer for Space THz Spectroscopy," *Proc. 16th Int. Symp. Space Terahertz Technol., May 2-4, 2005, Gothenburg, Sweden*, 543-548.

[23] B.S. Karasik, A.V. Sergeyev, D. Olaya, J. Wei, M.E. Gershenson, J.H. Kawamura, and W.R. McGrath, "A Photon Counting Hot-Electron Bolometer for Space THz Spectroscopy," *Proc. 16th Int. Symp. Space Terahertz Technol., May 2-4, 2005, Gothenburg, Sweden*, 543-548.

[24]. K.D. Irwin, "An application of electrothermal feedback for high resolution cryogenic particle detection," *Appl. Phys. Lett.* 66, 1998-2000 (1995).